Air-water CO_2 fluxes in a highly heterotrophic estuary.

Susana Flecha, I. Emma Huertas, Gabriel Navarro, Edward P. Morris and Javier Ruiz.

Instituto de Ciencias Marinas de Andalucía, Consejo Superior de Investigaciones Científicas (ICMAN-CSIC), Polígono Río San Pedro, Puerto Real, 11510, Cádiz, Spain.

1. Introduction

Estuaries, due to their transition location, are affected by both marine processes, such as tides, waves, intrusion of saline water, and riverine processes like flows of freshwater and sediments. They also represent an important source of nutrients to the coastal area, as estuarine systems are considered regions of a high productivity worldwide (Mann 1982). Nutrient inputs in estuaries (particularly nitrate) are affected by water discharge, entries from both natural (groundwater transport, riverine inflow and atmospheric deposition) and anthropogenic sources (sewage treatment plants, agricultural and lawn fertilizers etc), and resident estuarine processes, such as denitrification and nitrification (Soetaert et al. 2006).

Elevated nutrients concentrations spur rapid phytoplankton growth and the occurrence of periodic microalgal blooms that eventually lead to the generation of considerable organic loads. Subsequent bacterial decomposition of this organic matter promotes oxygen depletion and thus hypoxic or anoxic zones may commonly appear in estuaries (Conley et al., 2009). The genesis of hypoxia can be traced by specific nitrogen compounds, as nitrification processes decrease oxygen concentration, and denitrification principally proceeds in suboxic conditions. Hypoxia in estuaries represents a common disturbance (Cox et al., 2009; Sharp, 2010) causing death of biota and catastrophic changes at the entire ecosystem level (Vaquer-Sunyer and Duarte, 2008). Not only organisms and their habitat result affected by hypoxia, but also the biogeochemical processes that control nutrient concentrations in the water column (Conley et al., 2009). Moreover, turbulence induced by the meeting of the downstream freshwater flow and the upstream tidal flow, and flocculation of material induced by the mixing of fresh and salt water, increase residence times of suspended particulate matter (SPM), forming maximum turbidity zones (MTZ), which are generally considered the most important regions in a tidally influenced estuary, where photosynthesis becomes strongly limited by light availability (Abril et al., 1999; Amann et al., 2012; Etcheber et al., 2007; Garnier et al., 2010; Herman and Heip, 1999). Heterotrophic activity is in turn enhanced ought to the high turbidity, resulting in a net mineralization of a major part of the particulate organic carbon (POC) (Gattuso et al., 1998). As a final consequence, high levels of CO_2 generated by degradation of dissolved and/or particulate organic carbon and by other anaerobic processes in addition to denitrification, such as sulphate reduction and in some anaerobic environments methanogenesis (Richey et al., 1988), are released to the atmosphere. This kind of estuaries act then as significant sources of CO_2 to the

atmosphere due to their net heterotrophic metabolic status (Frankignoulle et al., 1998; Chen and Borges, 2009; Laruelle et al., 2010; Borges and Abril, 2011; Chen et al., 2012; Chen et al., 2013; Testa et al., 2013).

Given the complexity of the biogeochemical processes involved in the heterotrophy of estuaries, integrated studies performed at a high spatio-temporal scale are needed to properly characterize the dynamics of these systems. Furthermore, in order to determine the contribution of estuaries to the CO_2 emissions and the horizontal fluxes of carbon, high resolution data with a proper degree of accuracy are required to obtain and provide precise estimates of the air-water CO_2 exchange in these environments.

Within this context, this work was aimed at examining the temporal and spatial variability of the carbon system parameters in the tidally dominated Guadalquivir estuary (SW Spain, Fig.1) in relation to the metabolic status of the system. Despite its socio-economic and environmental significance (Ruiz et al., 2009), until very recently only one study addressing the characterization of the inorganic carbon system inside the estuary had been published (de la Paz et al., 2007). On other hand, several works have been carried out in the adjacent coastal fringe of the Gulf of Cádiz, where the Guadalquivir river discharges (Huertas et al., 2006; Ribas-Ribas et al., 2013) or in the wetlands of Doñana National Park, located in the northern rim of the lower estuary (Morris et al., 2013). The Guadalquivir estuary is characterized by a strong turbidity (Navarro et al., 2011; Caballero et al., 2013), which markedly restricts light availability for phytoplankton growth (Navarro et al., 2012). Light limitation seems to be a constant feature within the estuary, thereby constraining primary productivity even though high nutrients loads are present in the water column (Navarro et al., 2012, Ruiz et al., 2014). The seasonal shift in hydrology from winter river-dominated (rainfall season) to tidally dominated flow is the main factor controlling the patterns of nutrients and suspended matter in the estuary (Diez-Minguito et al., 2012), as during the river-dominated period considerable freshwater inputs from an upstream reservoir (the Alcala del Rio dam) are introduced in the system. Due to the relevance of the estuary on its adjacent areas, we assessed the spatio-temporal distribution of carbon system parameters in the system during nearly two years of sampling in relation to biogeochemical variables indicative of heterotrophy. The analysis was ultimately aimed at determining the air-water CO_2 exchange in the estuary and the processes governing gas transference.

2. Material and methods

77 2.1. Study area

78 The Guadalquivir River, located in Southern Spain (Fig.1), is one of the longest rivers in the Iberian
79 Peninsula, with a total length of 560 Km and a drainage area of 57,527 km^2. The estuarine region hosts
80 1.7 million inhabitants, which are distributed on 90 population settlements (Navarro et al., 2012). Due to
81 the socio-economic importance of the estuary (agriculture, fisheries, tourism, etc.), it is affected by an
82 intense anthropogenic pressure. Guadalquivir is the only large navigable river in Spain, reaching to the
83 port of Sevilla. Therefore, maintenance activities of the navigation channel take part regularly in the
84 estuary, including locks building and dredging works to deepen the main channel, in order to allow big
85 ships the access into Seville'sport (Ruiz et al., 2014).

86 The estuary extends to the Alcala del Rio dam, which is situated 110 km upstream from the river mouth,
87 being characterized by a main channel surrounded by tidal creeks with a few significant little intertidal
88 zones. As a mesotidal system, the tidal influence is noticeable up to the dam and the maximum tidal range
89 at river mouth is 3.5 m during spring tides (Díez-Minguito et al., 2012).

90 The basic climate in the region is Mediterranean, defined by warm temperatures (16.8°C annual average)
91 and with relatively short periods of heavy rainfall occurring during winter (annual average of 550 l m^{-2}).
92 The Atlantic Ocean orientation allows storms entering from West, driving the distribution of rainfall SW-
93 NE. The rainfall often adopts torrential character acting on a system recurrently affected by long dry
94 periods, high temperatures and consequently with a marked erosion susceptibility (Memoria de la
95 Confederación Hidrográfica del Guadalquivir 2009/2011, Ministerio de Agricultura, Alimentacion y
96 Medioambiente, Gobierno de España).

97 **2.2 Sampling strategy**

98 Monthly samplings were carried out at 12 stations between November 2007 and August 2009 (Fig.1).
99 From station 1 positioned at the river mouth, stations 2 to 12 were located at 6, 16, 22, 25, 34, 46, 55, 63,
100 71, 78 and 82 Km upstream, respectively. At each station, a CTD (Conductivity, Temperature and Depth),
101 salinity and turbidity profiles were obtained with a SeaBird SBE 19 plus equipped with a Turbidimeter
102 Cyclops-7sensor (Turner Designs), which was followed by collection of water samples at 1 m depth with
103 a Van Dorn Bottle Sampler for determination of the following biogeochemical variables: Total alkalinity

(A_T), pH, dissolved oxygen (DO), suspended particulate matter (SPM), chlorophyll (Chl*a*), inorganic nutrients (NH_4^+, NO_2^-, NO_3^-, PO_4^{-3} and Si), dissolved organic carbon (DOC) and total dissolved nitrogen (TDN).

2.3 Measurements protocols

Water samples for A_T determination were collected in 500 ml borosilicate bottles and poisoned with 100 µl of $HgCl_2$ saturated aqueous solution until analysis in the laboratory according to the DOE handbook protocols (Dickson and Goyet, 1994).A_T was measured by potentiometric titration with a Metrohm 794 Titroprocessor using the method described by Mintrop et al. (1999). The precision and accuracy of A_T determinations were between ±5.3 and 2.1 µmolkg^{-1}respectively, as determined from daily measurements of 2 batches (#94 and #97, n=44) of certified reference material (CRM, supplied by Prof. Andrew Dickson, Scripps Institution of Oceanography, La Jolla, CA, USA). Constants used for A_T calculations as for boric acid and $KHSO_4$ were those from Cai and Wang (1998), Lee et al. (2010) and Dickson (1990b), respectively. Water pH measurements in NBS (National Bureau of Standards) scale (pH_{NBS}) were carried out from the A_T samples using a Metrohm 780 pH meter equipped with a combined glass electrode. Calibrations were conducted daily using NBS buffers at three different pH values, 4, 7 and 9. Precision and accuracy of the pH measurements were 0.001 and ±0.003 pH units, respectively.

Dissolved oxygen was measured using an automated potentiometric modification of the original Winkler method following WOCE standards (WOCE, 1994.). Flasks containing the water samples were sealed, stored in darkness and measured within 24h. Dissolved oxygen concentrations were derived using a Metrohm 794 Titroprocessor, with an estimated error of ± 2 µmol l^{-1} (*n*=115).

SPM as well as particulate organic matter (POM) and particulate inorganic matter (PIM) were determined by using the Loss On Ignition (LOI) method. A known volume of water was filtered through pre-combusted 450º C Whatman GF/F glass fiber (0.7 mm pore size). Filters were dried at 60ºC for 48 h and weighed to derive SPM (g l^{-1}), further combusted at 450ºC for 5h and weighed to derive PIM and POM by difference.

Chlorophyll analysis was conducted by filtering known volumes of water through Whatman GF/F glass fiber filters, extracting in 90 % acetone overnight in the dark, and measuring chlorophyll a concentrations

(Chl*a*) by fluorometry with a Turner Designs 10-AU Model fluorometer according to the JGOFS protocol (Knap et al., 1996b) . The fluorometer was calibrated using a pure Chl*a* standard from the cyanobacterium *Anacystis nidulans* (Sigma Chemical Company).

Inorganic nutrients sampling was performed following the methodology described by Knap et al. (1996a). Two 5 ml samples of filtered water (Whatman GF/F glass fiber) were obtained and stored at -20ºC until analysis. Concentrations of NH_4^+, NO_2^-, NO_3^-, PO_4^{-3} and Si were derived following the techniques described by Grasshoff et al. (1983) using a Skalar San++ 215 Continuous Flow Analyzer. For the analysis of DOC and TDN, water samples were collected in borosilicate vials (pre-acid-washed and-combusted, 450ºC). Water was filtered with pre-combusted 450ºC Whatman GF/F glass fiber 47 mm filters and 24 ml sub-samples were acidified with 50 µl of 25% H_3PO_4, sealed and conserved at 4ºC in darkness until analysis. Samples for DOC and TDN were obtained according a modification of the JGOFS protocol (Knap et al., 1996a). Concentrations of DOC and TDN were derived by catalytic oxidation at high temperature (720ºC) and chemiluminescence, respectively using a Shimadzu TOC-VCPH analyser TDN was subsequently used to obtain Dissolved organic Nitrogen (DON) concentrations by subtracting inorganic nitrogen (Álvarez-Salgado and Miller, 1998).

The diffuse attenuation coefficient for photosyntetically active radiation (PAR) was calculated by the following expression obtained from Gallegos (2001):

$$K_d = K_w + K_c\,[\text{Chl}a] + K_s\,[\text{SPM}] \quad (1)$$

where K_W (0.26 m^{-1}) is the attenuation due to water alone, and K_C (0.017, (m^2 (mg Chl)$^{-1}$) and K_S (0.074 m^2 gr^{-1}), stand for the specific-attenuation coefficient of chlorophyll and SPM, respectively. The diffuse attenuation coefficient (K_d) was used to estimate the lower limit of the euphotic zone ($Z_{1\%}$) defined as the depth where the PAR represents 1% of the surface radiation, following the Lambert-Beer law (Kirk, 1994):

$$Z_{1\%} = \text{Ln}\,(0.01) / K_d \quad (2)$$

Calculations of air-water CO_2 fluxes

For fluxes calculations, $[pCO_2]_{water}$ and dissolved inorganic carbon (DIC) were obtained from A_T and pH_{NBS} pairs by using the CO2SYS software(Lewis et al., 1998) with the thermodynamic equations and constants for carbon and sulphate of Cai and Wang (1998) and Dickson (1990) respectively.

Air-water CO_2 fluxes (FCO_2 in $mmolCO_2\ m^{-2}\ d^{-1}$) were calculated according to Wanninkhof et al. (2009):

$$FCO_2 = k_w\ k_0\ ([pCO_2]_{water} - [pCO_2]_{air}) \quad (3)$$

where, k_w ($m\ s^{-1}$) is the water–side gas transfer velocity, k_0 ($mol\ m^{-3}\ atm^{-1}$) is the aqueous-phase solubility of CO_2 at the *in situ* temperature (ºC) and salinity (Weiss 1974; Wanninkhof 1992), and $[pCO_2]_{air}$ in µatm is the atmospheric pCO_2 values obtained from the NOAA Lampedusa (Italy) monitoring station (http://www.esrl.noaa.gov/gmd/dv/site/) and then converted from pCO_2dry to wet (Weiss and Price, 1980). k_w was calculated using:

$$k_w = k_{600}\ (S_{cw}/600)^{-0.5} \quad (4)$$

where, S_{cw} is the Schmidt number interpolated at the *in situ* salinity from the freshwater and sea water equations (see Wanninkhof, 1992). k_{600} is the gas transfer velocity at a Schmidt number of 600 (often quoted as typical of freshwater at 20ºC). k_{600} was predicted from time–ensemble averaged (1 d) horizontal wind velocity at 10 m above the surface ($U_{10}m\ s^{-1}$) using the empirical relationships of Raymond and Cole (2001),

$$k_{600} = 1.58\ e^{0.3}\ U_{10} \quad (5)$$

where k_{600} is in $cm\ h^{-1}$. U_{10} was calculated from U_z measured at nearby meteorological stations (Estaciones Agroclimaticas, Junta de Andalucia, Spain; Fig. 1) according to Smith (1988). For comparison, k_{600} proposed by Clark et al. (1995) and the recently revised by Jiang et al. (2008) were also used.

Daily discharge data from the Alcala del Rio dam and precipitation from the Lebrija Brazo del Este Station (Precipitation station in Fig.1) were obtained from the Sistema Automático de Información Hidrológica of the Guadalquivir basin (http://www.chguadalquivir.es/saih/Inicio.aspx).

Statistics

Statistics were performed with the statistical program language R 3.02 (R Development Core Team, 2013). Probability distributions of variables were examined visually and in most cases were log-normal and highly skewed. Non-parametrical Kruskal-Wallis rank sum tests (KWRS, R function; kruskal.test) and non-parametrical multiple test procedures (KWMC, Package; pgirmess, function; kruskalmc) were used to examine differences between zones (Giradoux, 2012). Significance levels were set at $p<0.05$. Principle components analysis (R package; FactoMineR, function; PCA, Husson et al., 2012) of transformed, log(x+1), variables, with monthly mean wind speed, monthly river discharge and surface temperature as a supplementary quantitative variables, was used to explore correlations. Linear regressions between variables were also used to establish linear relationships.

3. Results and discussion

Estuary partitioning: spatio-temporal distribution of thermohaline properties

PCA revealed that data could be summarised into 5 components that accounted for a cumulative percentage variance of 77% (Fig. 2), with values from PC1 to PC5 of 30.73, 19, 11.54, 8.75 and 6.63%, respectively. In terms of briefly characterising, only principle components 1 (PC1, Dim 1) and 2 (PC2, Dim 2) are discussed here. PC1 appears to represent spatial distribution and thus led us to divide the estuary in 3 regions. Positive PC1 values mainly represented higher values of dissolved material (A_T, DOC, and DON) corresponding to stations 9 to 12 (Fig. 1), which then defined the Inner Estuary (IE). Negative PC1 appears to represent elevated values of salinity, DO and pH corresponding to stations 1 and 2 (Fig. 1), characterizing hence the Lower Estuary (LE). The transitional zone between the inner and lower estuary, comprising stations 3 to 8 (Fig. 1), was then designed as the Middle Estuary (ME). IE was characterized by the presence of the lowest dissolved oxygen concentrations (Fig. 3) representing thus the Oxygen Minimum Zone (OMZ). During our study, oxygen levels were as low as 1.1 mg l^{-1} (Table 1), suggesting that OMZ can, at times, be classified as severely hypoxic. As defined by the Environmental Protection Agency (EPA, 2000), hypoxia in aquatic ecosystems occurs at oxygen levels below 2.9 mg l^{-1}, with severe hypoxia being marked by concentrations <2.3 mg l^{-1}. In contrast, oxygen levels in the ME and LE were ~ 6 mg l^{-1}in both zones.

208 Salinity range in the IE was mesohaline, with salinity values < 5 (Fig. 3 and Table 1), which
209 progressively increased throughout the estuary to finally reach 36 in the river mouth (LE, Fig. 3). The
210 spatial distribution of salinity within the entire estuary may be attributed to the combination between the
211 tidal flooding and variability in river discharge from the dam (Navarro et al., 2012, Díez-Minguito et al.,
212 2013).

213 In addition to salinity linked to PC1, turbidity was also selected as a variable defining spatial variability,
214 due to its relevance on the ecosystem dynamics (Navarro et al., 2012, Ruiz et al., 2014). Turbidity
215 maximum was located within the ME, defining the Maximum Turbidity Zone (MTZ) (Fig. 3 and Table
216 1).

217 On the other hand, PC2 seems to describe seasonal variations during the study period, as negative values
218 represent high temperature and Chl*a*, both mostly appearing during spring-summer (Fig 2). Conversely,
219 positive values define autumn-winter conditions with increased precipitations and particulate matter (PM)
220 contents. The highest spatial variability was found invariably in the ME, whereas at a temporal scale
221 spring season seemed to be the most fluctuating period for the whole estuary (Fig. 2).

222 Surface water temperature pattern was typical of the Mediterranean climate area, with hot summers and
223 moderate cold winters. During the study period, water temperature values ranged from 4.6 to 27.7ºC
224 (Table 1), with no statistical differences between zones (KWRSχ^2= 2.2, df (degrees of freedom) =2, *p*-
225 value > 0.05).In contrast, neither salinity nor dissolved oxygen values presented any seasonal variation
226 (KWRS *p*-value > 0.05).

227 *Chlorophyll, turbidity, water discharge and light penetration*

228 Guadalquivir estuary can be categorized as one of the most turbid rivers in the world, with average SPM
229 values of 650.5 mg l^{-1}(Table 1). For instance, rivers such as Huanghe (China), Mackenzie River (Canada),
230 Amazon (Brazil) and the Scheldt estuary (Belgium) have mean SPM concentrations of 23, 830, 320, 97
231 and 100 mg l^{-1} (Gaillardet et al., 1999; Kim et al., 2010; Chen et al., 2005), respectively. This is also
232 shown by the turbidity values provided by the CTD sensor (Table 1), which markedly varied along the
233 different zones of the estuary (KWRS, χ^2 = 63.1, df= 2, *p*-value < 0.001). The high turbidity in the

234 Guadalquivir estuary can be related to the generally long residence time and with the occurrence of high
235 mesotidal currents (Díez-Minguito et al., 2012; 2013).

236 As illustrated in Figure 4B, K_d values manifestly changed throughout the year (KWRS χ^2= 39.1, df=3, *p*-
237 value < 0.001), with a maximum of 400 m^{-1} reached in spring 2009 and a minimum of 1.5 m^{-1} in autumn
238 2008, resulting in changes in the euphotic depth from -0.01 to -3.1 m^{-1} (Fig. 4 C) . Maximum K_d values
239 where generally observed during periods of high precipitation or high discharges from the Alcala del Rio
240 dam (Fig. 4 A, B).When high loadings occurred, light penetration was more limited and hence the lower
241 limit of the euphotic zone shallowed (Fig.4B). As a result, primary production was expected to be highly
242 restricted due to reduced light availability and as seen also in Taglialatela et al. (2014) zooplankton
243 dominant species decreased to extremely low values during this events.

244 Chl*a* appeared to exhibit a seasonal trend (Fig. 4 D), with spring blooms in 2008 and 2009 with maxima
245 of 10µg l^{-1} and the lowest concentrations around 0.1 µg l^{-1}during autumn and winter coinciding with
246 increased precipitations and discharges. Nevertheless, Chl*a* concentrations were lower than the expected
247 phytoplankton biomass that could be supported by the nutrient levels present in the estuary (Ruiz et al.,
248 2014), feature that can be attributed to light limitation, as shown by the K_d and $Z_{1\%}$values, which indicate
249 that light penetrated on average only 5% into the water column.

250 *Carbon system parameters*

251 Total Alkalinity, plotted in Figure 5, was characterized by a marked spatial variability (KWRS χ^2= 83.5,
252 df=2, *p*-value <0.001), with the highest values measured being associated with the transition between IE
253 and ME (KWMC $p<0.05$). Minimum A_T concentrations were found in the LE, as the proximity to the
254 coastal area allows the inflow of seawater characterized by a lower A_T. In fact, in this part of the estuary,
255 the mean alkalinity during the whole study period was 2632.52±272.82 µmol kg^{-1}(Table 1), similar to that
256 measured in the continental shelf of the Gulf of Cádiz and equivalent to 2402.5±8 and 2360±2 (Ait-
257 Ameur and Goyet, 2006; Flecha et al., 2012). In contrast, waters with higher alkalinity were found
258 upstream, with average values of 3468.18±403.15 and 3505.33±327.98 µmolkg^{-1} in the ME and IE,
259 respectively. As reported previously by de la Paz et al. (2007), this alkalinity pattern can be partially
260 related to the carbonate materials presented in the drainage basin of the upper part of the estuary (Pérez-

261 Hidalgo and Trinidad, 2004) and the mixing between fresh and marine waters. A_T values did not present
262 any seasonal variation during the study period (Table 2).

263 The distribution of pH_{NBS} values also exhibited a strong spatial (KWRS χ^2= 95, df=2, *p*-value <0.001)
264 and temporal variability (KWRS χ^2= 48.6, df=2, *p*-value <0.001). No statistical differences were
265 observed (KWMC $p<0.05$) between spring and autumn whereas significant differences were found
266 among the rest of seasons, with winter being the period in which lower pH_{NBS} values were measured
267 (Table 2). The spatial variability of pH_{NBS} in the IE (Table 1, Fig. 5b) can be associated to the freshwater
268 discharges from the dam. Conversely, higher pH_{NBS} values found in the LE may reflect the entry of saltier
269 and oxygenated waters as well the influence of the DIC fluxes from the river. In opposition, pCO_2
270 exhibited a gradual increasing gradient upstream (Fig. 5C), as seen in other estuaries (Chen et al., 2012)
271 and already reported in this system (de la Paz et al., 2007). Extremely high pCO_2 concentrations (between
272 4000-5000 µatm) were detected in the IE, where pCO_2 levels always exceeded 1000 µatm during the
273 whole study period (Fig. 5c). In the LE, average values also coincide with those measured in previous
274 studies in the area (de la Paz et al., 2007; Ribas-Ribas et al., 2011), presenting during certain short
275 periods, pCO_2 values below the atmospheric concentration (Table 1). Nevertheless, our data show that the
276 Guadalquivir estuary, in average, was constantly characterized by pCO_2 values higher than the
277 atmospheric concentration. These CO_2 concentrations are higher in relation to those observed in the past,
278 which fell within a range from 518 to 3606 µatm from low to high salinity (de la Paz et al., 2007).

279 Taking salinity as a good indicator for mixing of dissolved compounds subject exclusively to physical
280 processes, a linear relationship between DIC and salinity can be obtained, which allows to estimate the
281 concentration of inorganic carbon in freshwater. Our calculations (DIC=3.68-0.034*S, r^2=0.64, n=248)
282 yield then a value of carbon in freshwater corresponding to 3.68 mmol kg^{-1} and considering a historic
283 average discharge of 160 m^3 s^{-1} (Ruiz, 2010), the transport of inorganic carbon by advective processes
284 from the Guadalquivir estuary to the continental shelf of the Gulf of Cádiz resulted in 50 x 10^6 mol C d^{-1},
285 indicating that the system has the potential to channelize an advective export of approximately 219,000
286 tons of C per year.

287 *Air-water CO_2 exchange*

Fluxes of CO_2 between the atmosphere and the water column (FCO_2) throughout the Guadalquivir estuary were calculated using three gas transfer velocities (k_{600}) for comparison. No large differences were detected between the outputs obtained with the parameterizations of Clark et al. (1995) and Raymond and Cole (2001), as k_{600} ranged from 2.54 to 7.26 and from 2.13 to 6.69 cm h^{-1}, respectively. In contrast, when the Jiang et al. (2008) parameterization was used, an increase in k_{600} was observed for the whole wind range (from 3.89 to 8.98 cm h^{-1}), as this formulation magnifies the coefficient values for wind speeds below 5 m s^{-1}. Taking into account this caveat and in order to compare with historic data, only fluxes calculated according to Raymond and Cole (2001) were subsequently considered in our study (Fig. 6).

The temporal distribution of FCO_2 indicated that estuarine waters were oversaturated with respect to the atmosphere during most of the study period (Fig. 6), with average annual FCO_2 values decreasing from 66.9±18.6 to 29.4±20.3 and to 3.4±8.1 mmol C m^{-2} d^{-1} in the IE, ME and LE, respectively (Table 3). Accordingly, the IE behaved as a strong CO_2 source to the atmosphere whereas the LE captured CO_2 during certain periods, particularly during the spring and summer months (Fig. 6). Overall, higher fluxes coincided with water discharges from the dam and increase in rainfall (Fig. 4A), although noticeable exchange variability was invariable found in the ME (Fig. 6). Nevertheless, CO_2 seasonal and annual fluxes were in the same order of magnitude than those measured in other estuarine areas and fall within the range compiled by Chen et al. (2013). In the Guadalquivir estuary in particular, the annual CO_2 flux from 2000 to 2003 calculated by using summer measurements along different sites of the estuary included now in the LE and ME of our division was 37.9 mol C $m^{-2}yr^{-1}$ (de la Paz et al., 2007). This value matches quite well that of 36.4±11.7 mol C $m^{-2}yr^{-1}$ obtained in our study for the whole system (Table 3). However, these authors also reported higher instant fluxes (around 114.3-128 mmol C m^{-2} d^{-1}) even though lower pCO_{2water} levels than those found here (Table 2) were present. This discrepancy may be mainly attributed to the average wind speeds, which were manifestly higher in the prior study (7.35 m s^{-1}) as compared to those measured during our sampling period (1.96 m s^{-1}), with less significance on the different k_{600} parameterizations used in both studies. Recently, Morris et al. (2013) provided FCO_2 at the adjacent Doñana wetlands fed by the Guadalquivir river that ranged from -4.1 to 5.5 mmol C m^{-2} d^{-1} and with a mean U_{10}value of 2.5 m s^{-1}, which are in the same order of magnitude than those computed at the LE adjacent to the Park (Fig. 6c and Table 3).

316 The pattern of both pCO_2 and air-water CO_2 exchange suggests that heterotrophy controls the metabolic
317 status of the estuarine waters. Thus, the strong correlation found between pCO_2 and the Apparent Oxygen
318 Utilization (AOU) (R^2=0.800, *p*-valor<0.001, Fig. 7) indicates that pCO_2 levels were mainly controlled by
319 biological processes, especially organic matter degradation. In the estuary, the organic carbon component
320 was significant, as indicated by the high DOC concentrations measured, with values varying from 1.5 to
321 14.5 mg l^{-1} (Table 1). No seasonality was found in the DOC levels (KWRS χ^2= 95, df=3, *p*-value <0.05)
322 although their spatial distribution revealed a clear variability (KWRS χ^2=31.6, df=2, *p*-value <0.001).
323 This finding reflects the effect of mixing as higher DOC concentrations were present upstream in fresh
324 water (Fig. 8) and a more dispersed pattern, with no statistical differences as in the case of turbidity, in
325 the IE and ME (KWMC *p*<0.05;Table 1). Using the criteria described by Abril et al. (2002), according to
326 the average DOC concentration (5.98±2.24 mgl^{-1}, *n*=184), and the considerable anthropogenic pressure
327 over the system (Ruiz et al., 2014), the Guadalquivir estuary can be categorized as heterotrophic and its
328 metabolic status is comparable to that of the Sado and Loire rivers. Another piece of evidence indicative
329 of the heterotrophic status is the inorganic nutrients levels present during the study period (Fig. 9), which
330 were also significantly different for each estuary zone (KWSR *p*<0.001). The highest concentrations of
331 nitrate, nitrite, ammonium and silicate were found in the IE and ME, with average values around 300, 6,
332 19 and 100 µM respectively (Table 1, Fig. 9), with a continue decrease towards the river mouth being
333 observed (Fig. 9). On the other hand, phosphate showed a more homogeneous spatial distribution (Fig. 9)
334 and average concentrations did not exceed 3 µM (Table 1). Seasonally, only nitrite and phosphate did not
335 present significant variations (KWRS *p*>0.05). Mendiguchía et al. (2007) reported lower nutrient content
336 in the system, particularly for NO_3^-, although sampling was performed twice a year and with river
337 discharges from the dam substantially lower than those observed during our study period.

338 The stoichiometric ratio N:P evidenced an excess of nitrogen in the system, as values were comprised
339 within the range of 173-1000, which is, on average, 12 times higher than the optimum Redfield ratio for
340 phytoplankton growth (Redfield 1934). The N:P ratios found here are of the same order of magnitude
341 than that observed in the Pearl River estuary and, in general, characteristic of systems that receive inputs
342 from inland waters enriched in nitrogen relative to phosphorus (Harrison et al., 2008).

343 In addition, other processes such as denitrification, could partially contribute to the nutrient content in the
344 estuary, particularly because denitrification is favoured in heavy turbid and nitrogen enriched waters,

345 even under oxic conditions (Liu et al., 2013). From ammonia and nitrate reduction, the nitrification-
346 denitrification process results in increased concentrations of the intermediate NO_2^-component under oxic
347 and anoxic conditions, respectively. Consequently, a rise in N_2O emissions to the atmosphere is
348 commonly observed. In the Guadalquivir estuary, concentrations of NO_3^-,NO_2^- and NH_4^+ in the ME
349 (MTZ) and the IE (OMZ), were significantly different from those in the LE (KWMC $p<0.05$) and
350 substantially higher (Table 1 and Fig. 9), which may be indeed indicative of an enhanced denitrifying
351 microbes activity. In addition, pH_{NBS} values in the IE (7.80±0.17, Table 1) would favour denitrification
352 (Soetaert et al., 2007) and the elevated A_T measured in this zone (Table 1) would also be indicative of the
353 presence of denitrification, as seen in other anoxic estuaries (Abril and Frankignoulle, 2001). Considering
354 that Ferrón et al. (2010) defined the coastal fringe connected to the Guadalquivir river mouth as a N_2O
355 source to the atmosphere and the highest nitrous oxide saturation concentrations were found at the lowest
356 salinity zone, denitrification may be well claimed as a relevant mechanism participating in the nitrogen
357 balance of the estuary. Nevertheless, further denitrification measurements are required to support this
358 conclusion.

359 **4. Summary**

360 Our work shows that the high turbid Guadalquivir estuary behaved as a net CO_2 source to the atmosphere
361 during a nearly two year period (2007-2009) and a low net gas absorption was only detected in the more
362 saline river mouth during short time intervals. Seasonal variations in the air-water CO_2 fluxes were
363 generally well correlated with an increase in the discharge/rainfall regime in the area, although the
364 permanent heterotrophy in the estuary was the main factor controlling the CO_2 levels in its waters. The
365 very high CO_2 concentrations found in the system and comparable to other high heterotrophic and turbid
366 estuaries were mainly due to the high organic matter and nutrient content (particularly nitrate), which
367 favours respiratory decomposition and denitrification. This status was reflected in a pronounced hypoxia
368 during certain periods and particularly in the inner zone of the estuary, which was also exacerbated by
369 limitation in light penetration, hampering phytoplankton growth and the concomitant water oxygenation.
370 Our data and comparisons with previous records reported in the area confirmed that the Guadalquivir
371 estuary acts as a permanent potent CO_2 emitter to the atmosphere.

372 **Acknowledgments**

We are grateful to the anonymous reviewers and associate editor for comments on the manuscript. This research was funded by the Andalusian Regional Government, by the project P09–RNM–4853 and by the Spanish Ministry of Agriculture, Food and Environment through the project 49/2010. Guidance and advice for fluxes calculations provided by Prof. Alberto Borges and his group is highly appreciated. SF was supported by a JAE PREDOCTORAL scholarship and a COST Action 735. EPM was supported by a JAE DOCTORES 2010 contract, both JAE are part-funded by the European Union (European Social Fund ESF2007-2013) and the Spanish Ministry for Economy and Competitiveness. Authors also thank Antonio Moreno, David Roque, Simone Taglialatela, Manuel Arjonilla, and María Ferrer-Marco for their assistance in samples collection and measurements.

References

Memoria 2009/2011, ed. C.H.d. Guadalquivir: Ministerio de Agricultura, Alimentación y Medio Ambiente, Gobierno de España.

Abril, G., H. Etcheber, P. Le Hir, P. Bassoullet, B. Boutier, and M. Franki-Gnoulle. 1999. Oxic/anoxic oscillations and organic carbon mineralization in an estuarine maximum turbidity zone (The Gironde, France). *Limnology and Oceanography* 44: 1304-1315.

Abril, G., and M. Frankignoulle. 2001. Nitrogen–alkalinity interactions in the highly polluted Scheldt basin (Belgium). *Water Research* 35: 844-850.

Abril, G., M. Nogueira, H. Etcheber, G. Cabeçadas, E. Lemaire, and M. Brogueira. 2002. Behaviour of organic carbon in nine contrasting European estuaries. *Estuarine, Coastal and Shelf Science* 54: 241-262.

Ait-Ameur, N., and C. Goyet. 2006. Distribution and transport of natural and anthropogenic CO_2 in the Gulf of Cadiz. *Deep-Sea Research Part Ii-Topical Studies in Oceanography* 53: 1329-1343.

395 Álvarez-Salgado, X.A., and A.E. Miller. 1998. Simultaneous determination of dissolved organic carbon
396 and total dissolved nitrogen in seawater by high temperature catalytic oxidation: conditions for
397 precise shipboard measurements. *Marine Chemistry* 62: 325-333.

398 Amann, T., A. Weiss, and J. Hartmann. 2012. Carbon dynamics in the freshwater part of the Elbe estuary,
399 Germany: Implications of improving water quality. *Estuarine, Coastal and Shelf Science* 107:
400 112-121.

401 Borges, A., and G. Abril. 2011. 5.04-Carbon Dioxide and Methane Dynamics in Estuaries. Treatise on
402 Estuarine and Coastal Science, Volume 5: Biogeochemistry.

403 Caballero, I., E.P. Morris, J. Ruiz, and G. Navarro. Assessment of suspended solids in the Guadalquivir
404 estuary using new DEIMOS-1 medium spatial resolution imagery. *Remote Sensing of*
405 *Environment*.

406 Cai, W.-J., and Y. Wang. 1998. The Chemistry, Fluxes, and Sources of Carbon Dioxide in the Estuarine
407 Waters of the Satilla and Altamaha Rivers, Georgia. *Limnology and Oceanography* 43: 657-668.

408 Clark, J.F., P. Schlosser, R. Wanninkhof, H.J. Simpson, W.S.F. Schuster, and D.T. Ho. 1995. Gas transfer
409 velocities for SF_6 and ^3He in a small pond at low wind speeds. *Geophysical Research Letters* 22:
410 93-96.

411 Conley, D.J., J. Carstensen, R. Vaquer-Sunyer, and C.M. Duarte. 2009. Ecosystem thresholds with
412 hypoxia. In *Eutrophication in Coastal Ecosystems*, 21-29: Springer.

413 Cox, T., T. Maris, K. Soetaert, D. Conley, S.V. Damme, P. Meire, J.J. Middelburg, M. Vos, and E.
414 Struyf. 2009. A macro-tidal freshwater ecosystem recovering from hypereutrophication: the
415 Schelde case study. *Biogeosciences* 6.

Chen, C.-T., T.-H. Huang, Y.-C. Chen, Y. Bai, X. He, and Y. Kang. 2013. Air–sea exchanges of CO 2 in the world's coastal seas. *Biogeosciences* 10: 6509-6544.

Chen, C.-T.A., and A.V. Borges. 2009. Reconciling opposing views on carbon cycling in the coastal ocean: Continental shelves as sinks and near-shore ecosystems as sources of atmospheric CO_2. *Deep Sea Research Part II: Topical Studies in Oceanography* 56: 578-590.

Chen, C.-T.A., T.-H. Huang, Y.-H. Fu, Y. Bai, and X. He. 2012. Strong sources of CO_2 in upper estuaries become sinks of CO_2 in large river plumes. *Current Opinion in Environmental Sustainability* 4: 179-185.

Chen, M., S. Wartel, B. Eck, and D. Maldegem. 2005. Suspended matter in the Scheldt estuary. *Hydrobiologia* 540: 79-104.

de la Paz, M., A. Gómez-Parra, and J.M. Forja. 2007. Inorganic carbon dynamic and air–water CO_2 exchange in the Guadalquivir Estuary (SW Iberian Peninsula). *Journal of Marine Systems* 68: 265-277.

Dickson, A.G. 1990a. Standard potential of the reaction: AgCl(s) + $12H_2$(g) = Ag(s) + HCl(aq), and and the standard acidity constant of the ion HSO_4^- in synthetic sea water from 273.15 to 318.15 K. *The Journal of Chemical Thermodynamics* 22: 113-127.

Dickson, A.G. 1990b. Thermodynamics of the dissociation of boric acid in synthetic seawater from 273.15 to 318.15 K. *Deep Sea Research Part A. Oceanographic Research Papers* 37: 755-766.

Dickson, A.G., and C. Goyet. 1994. Handbook of methods for the analysis of the various parameters of the carbon dioxide system in sea water. Version 2: Oak Ridge National Lab., TN (United States).

436 Díez-Minguito, M., A. Baquerizo, M. Ortega-Sánchez, G. Navarro, and M.A. Losada. 2012. Tide
437 transformation in the Guadalquivir estuary (SW Spain) and process-based zonation. *Journal of*
438 *Geophysical Research: Oceans* 117: C03019.

439 Díez-Minguito, M., E. Contreras, M.J. Polo, and M.A. Losada. 2013. Spatio-temporal distribution, along-
440 channel transport, and post-riverflood recovery of salinity in the Guadalquivir estuary (SW
441 Spain). *Journal of Geophysical Research: Oceans* 118: 2267-2278.

442 Etcheber, H., A. Taillez, G. Abril, J. Garnier, P. Servais, F. Moatar, and M.-V. Commarieu. 2007.
443 Particulate organic carbon in the estuarine turbidity maxima of the Gironde, Loire and Seine
444 estuaries: origin and lability. *Hydrobiologia* 588: 245-259.

445 Ferrón, S., T. Ortega, and J.M. Forja. 2010. Nitrous oxide distribution in the north-eastern shelf of the
446 Gulf of Cádiz (SW Iberian Peninsula). *Marine Chemistry* 119: 22-32.

447 Flecha, S., F.F. Pérez, G. Navarro, J. Ruiz, I. Olivé, S. Rodríguez-Gálvez, E. Costas, and I.E. Huertas.
448 2012. Anthropogenic carbon inventory in the Gulf of Cádiz. *Journal of Marine Systems* 92: 67-
449 75.

450 Frankignoulle, M., G. Abril, A. Borges, I. Bourge, C. Canon, B. Delille, E. Libert, and J.-M. Théate.
451 1998. Carbon dioxide emission from European estuaries. Science 282: 434-436.

452 Gaillardet, J., B. Dupré, and C.J. Allègre. 1999. Geochemistry of large river suspended sediments: silicate
453 weathering or recycling tracer? *Geochimica et Cosmochimica Acta* 63: 4037-4051.

454 Gallegos, C.L. 2001. Calculating optical water quality targets to restore and protect submersed aquatic
455 vegetation: overcoming problems in partitioning the diffuse attenuation coefficient for
456 photosynthetically active radiation. *Estuaries* 24: 381-397.

457 Garnier, J., G. Billen, J. Némery, and M. Sebilo. 2010. Transformations of nutrients (N, P, Si) in the
458 turbidity maximum zone of the Seine estuary and export to the sea. *Estuarine, Coastal and Shelf*
459 *Science* 90: 129-141.

460 Gattuso, J.P., M. Frankignoulle, and R. Wollast. 1998. Carbon and Carbonate Metabolism in Coastal
461 Aquatic Ecosystems. *Annual Review of Ecology and Systematics* 29: 405-434.

462 Giradoux, P. 2012. pgirmess: Data analysis in ecology. R package version 1.5.4. http://CRAN.R-
463 project.org/package=pgirmess.

464 Grasshoff, K., M. Erhardt, and K. Kremling. 1983. Methods of Seawater Analysis. 2. *Acta hydrochimica*
465 *et hydrobiologica* 14: 79-80.

466 Harrison, J.A., R.J. Maranger, R.B. Alexander, A.E. Giblin, P.A. Jacinthe, E. Mayorga, S.P. Seitzinger,
467 D.J. Sobota, and W.M. Wollheim. 2009. The regional and global significance of nitrogen
468 removal in lakes and reservoirs. *Biogeochemistry* 93: 143-157.

469 Herman, P.M., and C.H. Heip. 1999. Biogeochemistry of the MAximum TURbidity Zone of Estuaries
470 (MATURE): some conclusions. *Journal of Marine Systems* 22: 89-104.

471 Huertas, I.E., G. Navarro, S. Rodríguez-Gálvez, and L.M. Lubián. 2006. Temporal patterns of carbon
472 dioxide in relation to hydrological conditions and primary production in the northeastern shelf of
473 the Gulf of Cadiz (SW Spain). *Deep Sea Research Part II: Topical Studies in Oceanography* 53:
474 1344-1362.

475 Husson, F., J. Josse, S. Le, and J. Mazet. 2012. FactoMineR: Multivariate exploratory data analysis and
476 data mining with R. In package= FactoMineR.R package version 1.19. http://CRAN.R-
477 project.org/

478 Jiang, L.-Q., W.-J. Cai, and Y. Wang. 2008. A Comparative Study of Carbon Dioxide Degassing in
479 River- and Marine-Dominated Estuaries. *Limnology and Oceanography* 53: 2603-2615.

480 Kim, T.W., K. Lee, R.A. Feely, C.L. Sabine, C.T.A. Chen, H.J. Jeong, and K.Y. Kim. 2010. Prediction of
481 Sea of Japan (East Sea) acidification over the past 40 years using a multiparameter regression
482 model. *Global Biogeochemical Cycles* 24.

483 Kirk, J.T.O. 1994. *Light and photosynthesis in aquatic ecosystems*: Cambridge university press.

484 Knap, A., A. Michaels, A. Close, H. Ducklow, and A. Dickson. 1996a. Protocols for the joint global
485 ocean flux study (JGOFS) core measurements. *JGOFS, Reprint of the IOC Manuals and Guides*
486 *No. 29, UNESCO 1994* 19.

487 Knap, A.H., A. Michaels, A.R. Close, H. Ducklow, and A.G. Dickson. 1996b. Protocols for the Joint
488 Global Ocean Flux Study (JGOFS) Core Measurements.

489 Laruelle, G.G., H.H. Dürr, C.P. Slomp, and A.V. Borges. 2010. Evaluation of sinks and sources of CO2
490 in the global coastal ocean using a spatially-explicit typology of estuaries and continental
491 shelves. *Geophysical Research Letters* 37.

492 Lee, K., T.-W. Kim, R.H. Byrne, F.J. Millero, R.A. Feely, and Y.-M. Liu. 2010. The universal ratio of
493 boron to chlorinity for the North Pacific and North Atlantic oceans. *Geochimica et*
494 *Cosmochimica Acta* 74: 1801-1811.

495 Lewis, E., D. Wallace, and L.J. Allison. 1998. *Program developed for CO2 system calculations*: Carbon
496 Dioxide Information Analysis Center, managed by Lockheed Martin Energy Research
497 Corporation for the US Department of Energy.

498 Liu, T., X. Xia, S. Liu, X. Mou, and Y. Qiu. 2013. Acceleration of Denitrification in Turbid Rivers Due to
499 Denitrification Occurring on Suspended Sediment in Oxic Waters. *Environmental Science &*
500 *Technology* 47: 4053-4061.

501 Mann, K.H. 1982. *Ecology of coastal waters: a systems approach*: Univ of California Press.

502 Mendiguchía, C., C. Moreno, and M. García-Vargas. 2007. Evaluation of natural and anthropogenic
503 influences on the Guadalquivir River (Spain) by dissolved heavy metals and nutrients.
504 *Chemosphere* 69: 1509-1517.

505 Mintrop, L., A. Kortzinger, and J.C. Duinker. 1999. The carbon dioxide system in the northwestern
506 Indian Ocean during south-west monsoon. *Marine Chemistry* 64: 315-336.

507 Morris, E.P., S. Flecha, J. Figuerola, E. Costas, G. Navarro, J. Ruiz, P. Rodriguez, and E. Huertas. 2013.
508 Contribution of Doñana Wetlands to Carbon Sequestration. *PLoS ONE* 8: e71456.

509 Navarro, G., F. Gutiérrez, M. Díez-Minguito, M. Losada, and J. Ruiz. 2011. Temporal and spatial
510 variability in the Guadalquivir estuary: a challenge for real-time telemetry. *Ocean Dynamics* 61:
511 753-765.

512 Navarro, G., I.E. Huertas, E. Costas, S. Flecha, M. Díez-Minguito, I. Caballero, V. López-Rodas, L.
513 Prieto, and J. Ruiz. 2012. Use of a real-time remote monitoring network (RTRM) to characterize
514 the Guadalquivir estuary (Spain). *Sensors* 12: 1398-1421.

515 Pérez-Hidalgo, T., and J. Trinidad. 2004. Cuencas cenozoicas. In *Geología de España*, ed. I.G.y.M.d.
516 España.

517 R Development Core Team. 2013. R: A language and enviroment for stadistical computing. Vienna,
518 Austria: R Foundation for Stadistical Computing.

519 Raymond, P., and J. Cole. 2001. Gas exchange in rivers and estuaries: Choosing a gas transfer velocity.
520 *Estuaries and Coasts* 24: 312-317.

521 Redfield, A.C. 1934. *On the proportions of organic derivatives in sea water and their relation to the*
522 *composition of plankton*: University Press of Liverpool.

523 Ribas-Ribas, M., E. Anfuso, A. Gómez-Parra, and J.M. Forja. 2013. Tidal and seasonal carbon and
524 nutrient dynamics of the Guadalquivir estuary and the Bay of Cádiz (SW Iberian Peninsula).
525 *Biogeosciences* 10: 4481-4491.

526 Ribas-Ribas, M., A. Gómez-Parra, and J.M. Forja. 2011. Air–sea CO< sub> 2</sub> fluxes in the north-
527 eastern shelf of the Gulf of Cádiz (southwest Iberian Peninsula). *Marine Chemistry* 123: 56-66.

528 Richey, J.E., A.H. Devol, S.C. Wofsy, R. Victoria, and M.N. Riberio. 1988. Biogenic gases and the
529 oxidation and reduction of carbon in Amazon River and floodplain waters. *Limnol. Oceanogr*
530 33: 551-561.

531 Ruiz, J. 2010. Capítulo 7: Ciclos biogeoquímicos del estuario: Impacto sobre la Biota, la Biodiversidad y
532 la Toxicidad. In Propuesta metodológica para diagnosticar y ponosticar las consecuencias de las
533 actuaciones humanas en el estuario del Guadalquivir., ed. A.P.d. Sevilla: Instituto de Ciencias
534 Marinas de Andalucia (ICMAN-CSIC).

535 Ruiz, J., R. González-Quirós, L. Prieto, and G. Navarro. 2009. A Bayesian model for anchovy (Engraulis
536 encrasicolus): the combined forcing of man and environment. *Fisheries Oceanography* 18: 62-
537 76.

538 Ruiz, J., M.J. Polo, M. Díez-Minguito, G. Navarro, E.P. Morris, E. Huertas, I. Caballero, E. Contreras,
539 and M.A. Losada. 2014. The Guadalquivir estuary: A hot spot for enviromental and human
540 conflicts. In *Advances in Coastal and Marine Resources: Remote Sensing and Modeling*, ed.
541 C.W. Finkl: Submitted.

542 Sharp, J.H. 2010. Estuarine oxygen dynamics: What can we learn about hypoxia from long-time records
543 in the Delaware Estuary? *Limnology and Oceanography* 55: 535.

544 Smith, S.D. 1988. Coefficients for sea surface wind stress, heat flux, and wind profiles as a function of
545 wind speed and temperature. *Journal of Geophysical Research: Oceans* 93: 15467-15472.

546 Soetaert, K., A.F. Hofmann, J.J. Middelburg, F.J.R. Meysman, and J. Greenwood. 2007. The effect of
547 biogeochemical processes on pH. *Marine Chemistry* 105: 30-51.

548 Soetaert, K., J.J. Middelburg, C. Heip, P. Meire, S. Van Damme, and T. Maris. 2006. Long-term change
549 in dissolved inorganic nutrients in the heterotrophic Scheldt estuary (Belgium, The Netherlands).
550 *Limnology and Oceanography* 51: 409-423.

551 Taglialatela, S., L. Prieto, G. Navarro, and J. Ruiz Segura. 2012. Annual patterns in mesozooplankton
552 distibution along the salinity gradient in the Guadalquivir Estuary. *Estuarine, Coastal and Shelf*
553 *Science* 149: 244-254.

554 Testa, J.M., W.M. Kemp, C.S. Hopkinson, and S.V. Smith. 2013. Ecosystem Metabolism. Estuarine
555 Ecology, Second Edition: 381-416.

556 Vaquer-Sunyer, R., and C.M. Duarte. 2008. Thresholds of hypoxia for marine biodiversity. *Proceedings*
557 *of the National Academy of Sciences* 105: 15452-15457.

558 Wanninkhof, R. 1992. Relationship between wind speed and gas exchange. *J. geophys. Res* 97: 7373-
559 7382.

560 Wanninkhof, R., W.E. Asher, D.T. Ho, C. Sweeney, and W.R. McGillis. 2009. Advances in Quantifying
561 Air-Sea Gas Exchange and Environmental Forcing. *Annual Review of Marine Science* 1: 213-
562 244.

563 Weiss, R., and B. Price. 1980. Nitrous oxide solubility in water and seawater. *Marine Chemistry* 8: 347-
564 359.

565 Weiss, R.F. 1974. Carbon dioxide in water and seawater: the solubility of a non-ideal gas. *Marine*
566 *Chemistry* 2: 203-215.

567

568 Table 1: Average values, standard deviation and number of observations in brackets (n) of the variables
569 presented in this study for the three areas defined in the Guadalquivir estuary.

570

571 Table 2: Average values, standard deviation and number of observations in brackets (n) of pH_{NBS} A_T
572 (µmol kg^{-1}), DIC (µmol kg^{-1}) and pCO_2 (µatm) in each season.

573

574 Table 3: Spatio-temporal FCO_2 average values and standard deviation.

575

576 Figure 1: Location of the study area, sampling sites and meteorological stations. Position of the Alcala del
577 Río dam is also shown.

578

579 Figure 2: Biplots of water physical and chemical characteristics with scaling highlighting variable
580 correlations (A) and mapping of individual samples (B). Rainfall, wind velocity and Alcala del Rio dam
581 discharge are plotted as supplementary variables (blue arrows and text) on A. Text representing the
582 centroids for Lower Estuary (LE), Middle Estuary (ME) and Inner Estuary (IE) and seasons are shown on
583 B.

584

585 Figure 3: Average values of salinity, dissolved oxygen (mg l^{-1}) and turbidity in Formazin Nephelometric
586 Units (FNU) along the estuary, defining the three areas in which the estuary has been divided: LE, ME
587 and IE.

588

589 Figure 4: Time distribution in the Guadalquivir estuary of: a) Daily averaged discharge (m^3 s^{-1}) in grey
590 and precipitation (l m^{-2}) dotted red, b) Light extinction coefficient, K_d (m^{-1}) c) Euphotic zone, $Z_{1\%}$ (m^{-1})
591 and d) Chlorophyll *a*, Chl*a* (µg l^{-1}). Grey background bands highlight the periods with higher discharges
592 in the estuary during the time of the study. The tops and bottoms of each "box" are the 25^{th} and 75^{th}

593 percentiles of the samples, respectively. The distances between the tops and bottoms are the interquartile
594 ranges. The line in the middle of each box is the sample median. Observations beyond the whisker length
595 are marked as outliers displayed with a black dot.

596

597 Figure 5: a) Total alkalinity (µmolkg^{-1}), b) pH (NBS scale), and c) pCO_2values (µatm) from the river
598 mouth to 80 Km upstream. The tops and bottoms of each "box" are the 25th and 75th percentiles of the
599 samples, respectively. The distances between the tops and bottoms are the interquartile ranges. The line in
600 the middle of each box is the sample median. Observations beyond the whisker length are marked as
601 outliers displayed with a black dot.

602

603 Figure 6: Spatio-temporal distribution of air-water CO_2 fluxes (FCO_2, mmol m^{-2} d^{-1}) in the Guadalquivir
604 estuary during the study period for the: A) IE, B) ME and C) LE. Negative FCO_2values indicate that the
605 area acts as a sink and positives as a source. The tops and bottoms of each "box" are the 25th and 75th
606 percentiles of the samples, respectively. The distances between the tops and bottoms are the interquartile
607 ranges. The line in the middle of each box is the sample median.

608

609 Figure 7: pCO_2 (µatm) values in relation to Apparent Oxygen Utilization (AOU) in the Guadalquivir
610 estuary.

611

612 Figure 8: Dissolved organic carbon (mg l^{-1}) in relation to salinity in the Guadalquivir estuary.

613

614 Figure 9: Average concentrations (µM) of inorganic nutrients: nitrate (NO_3^-), nitrite (NO_2^-), ammonium
615 (NH_4^+), phosphate (PO_4^{3-}), and silicate (Si) from the river mouth to 80 upstream during the period of
616 study. The tops and bottoms of each "box" are the 25th and 75th percentiles of the samples, respectively.
617 The distances between the tops and bottoms are the interquartile ranges. The line in the middle of each

box represents the sample median. Observations beyond the whisker length are marked as outliers displayed with a black dot.

Figure1
Click here to download high resolution image

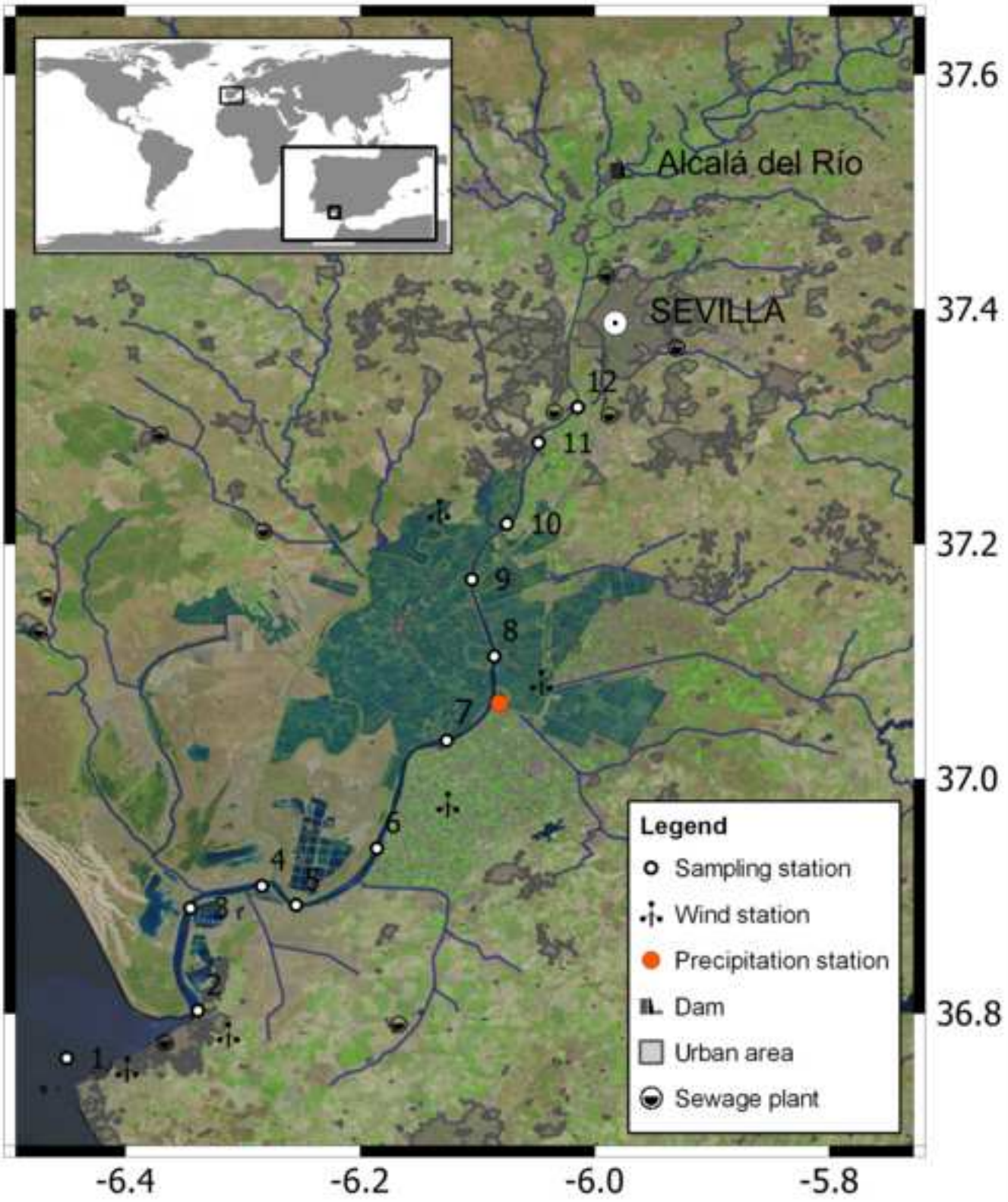

Figure2
Click here to download high resolution image

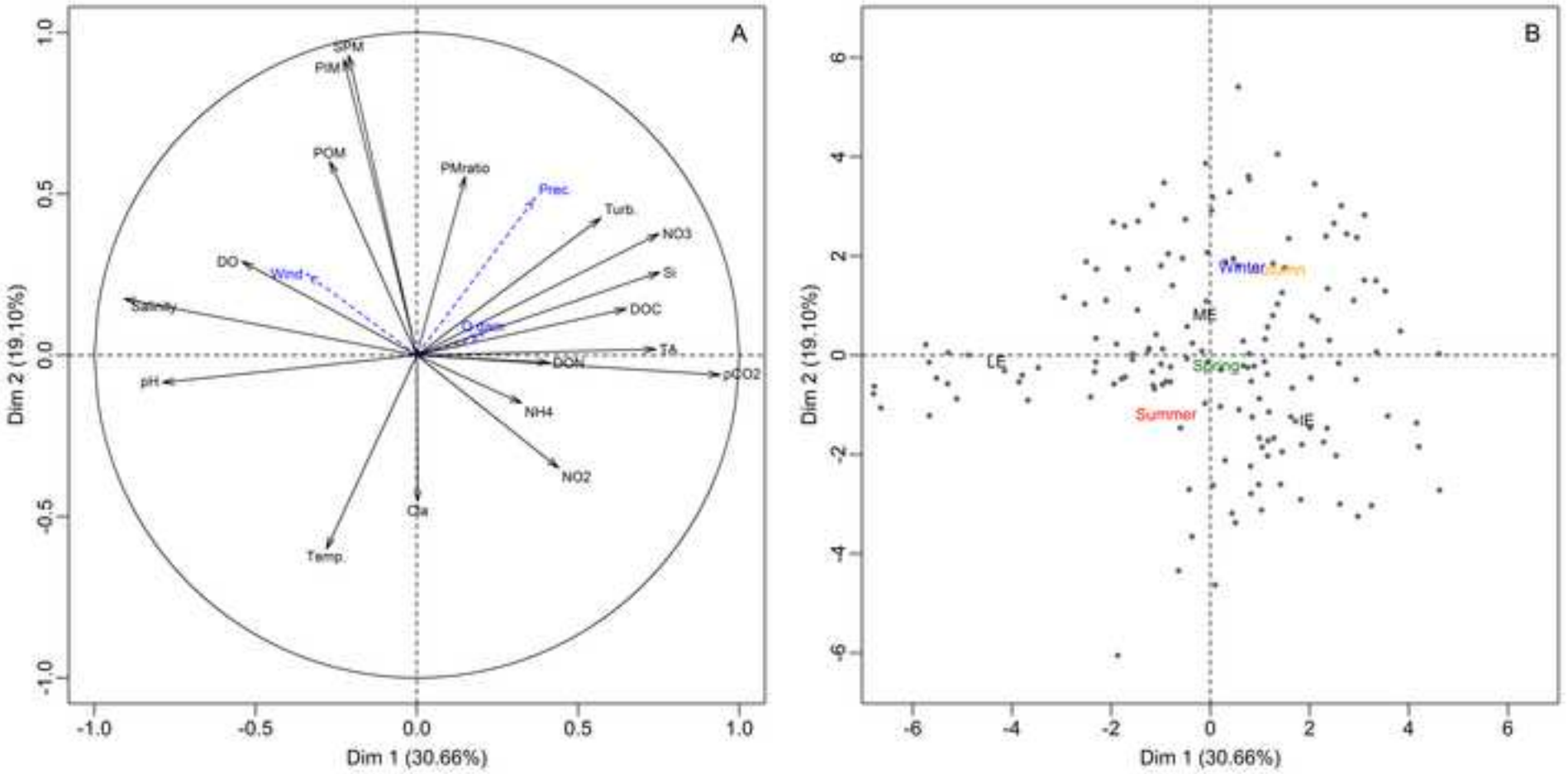

Figure3
Click here to download high resolution image

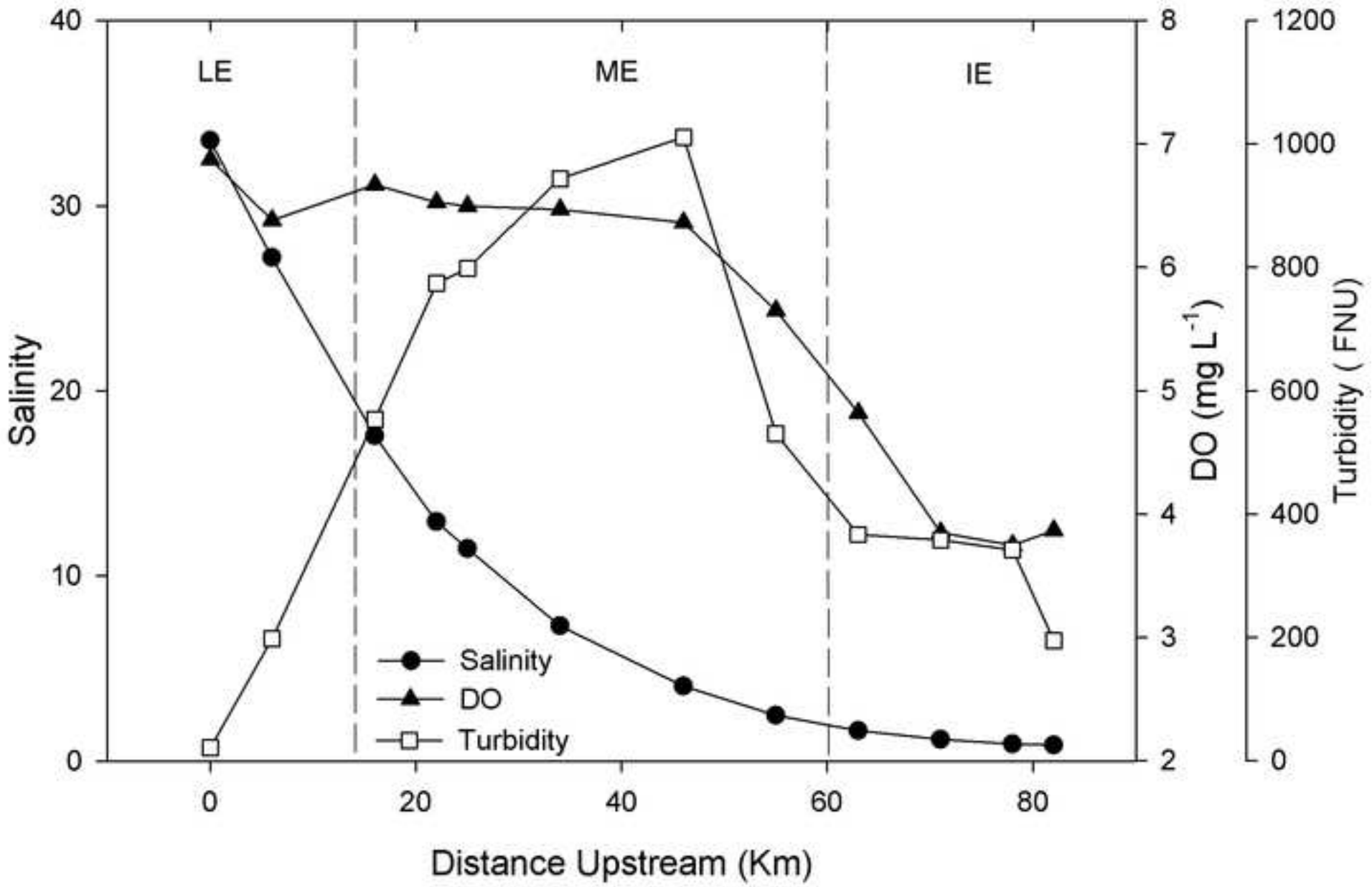

Figure4
Click here to download high resolution image

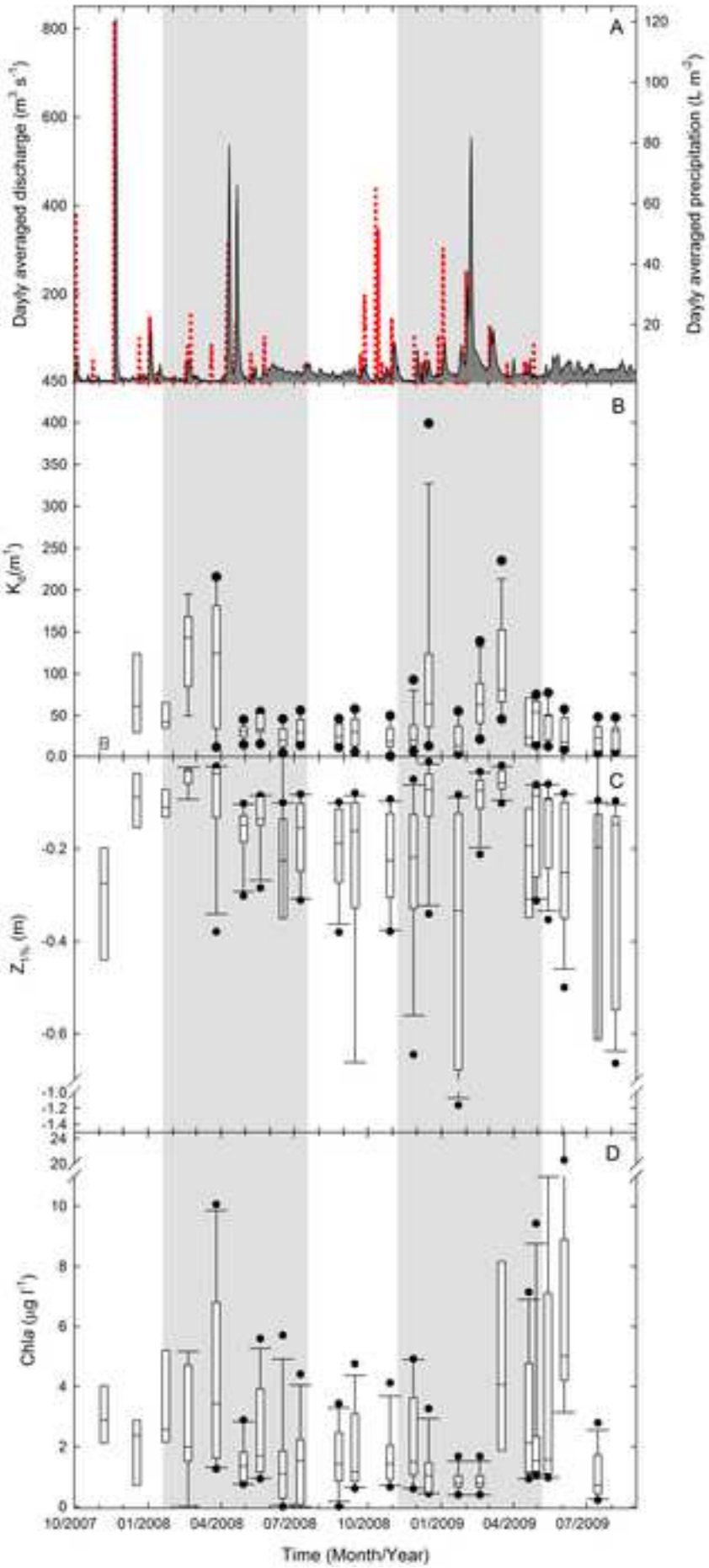

Figure5
Click here to download high resolution image

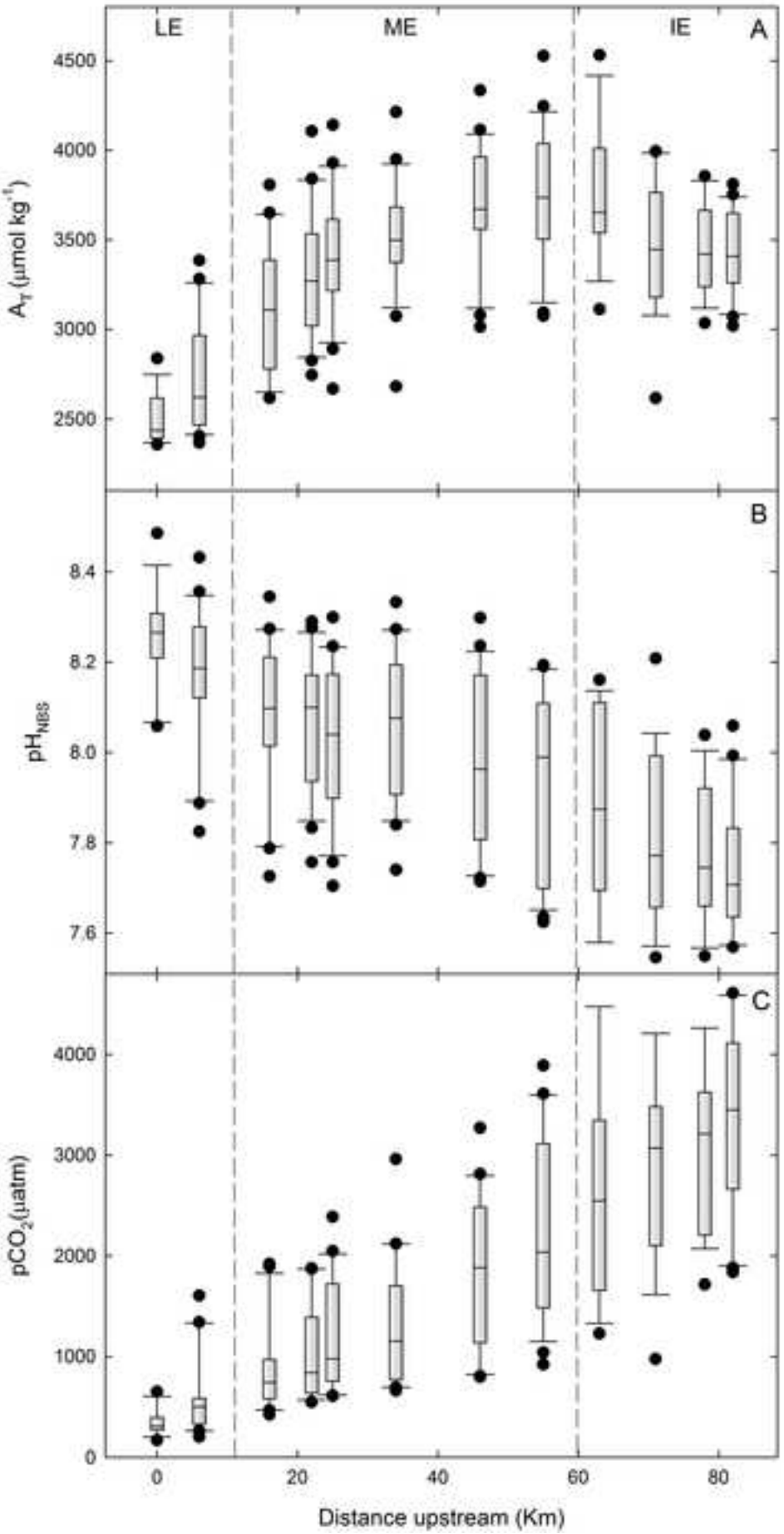

Figure6
Click here to download high resolution image

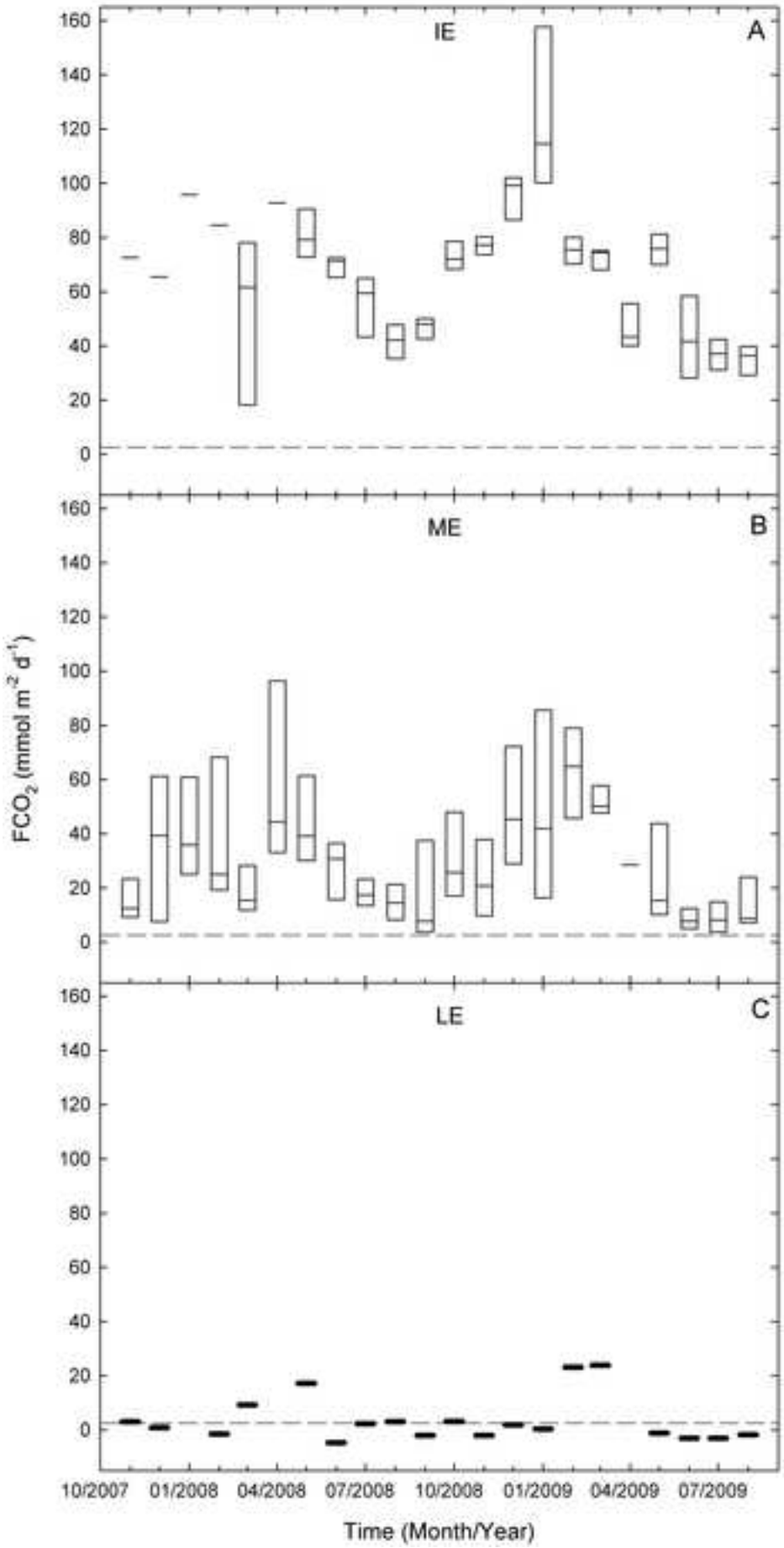

Figure7
Click here to download high resolution image

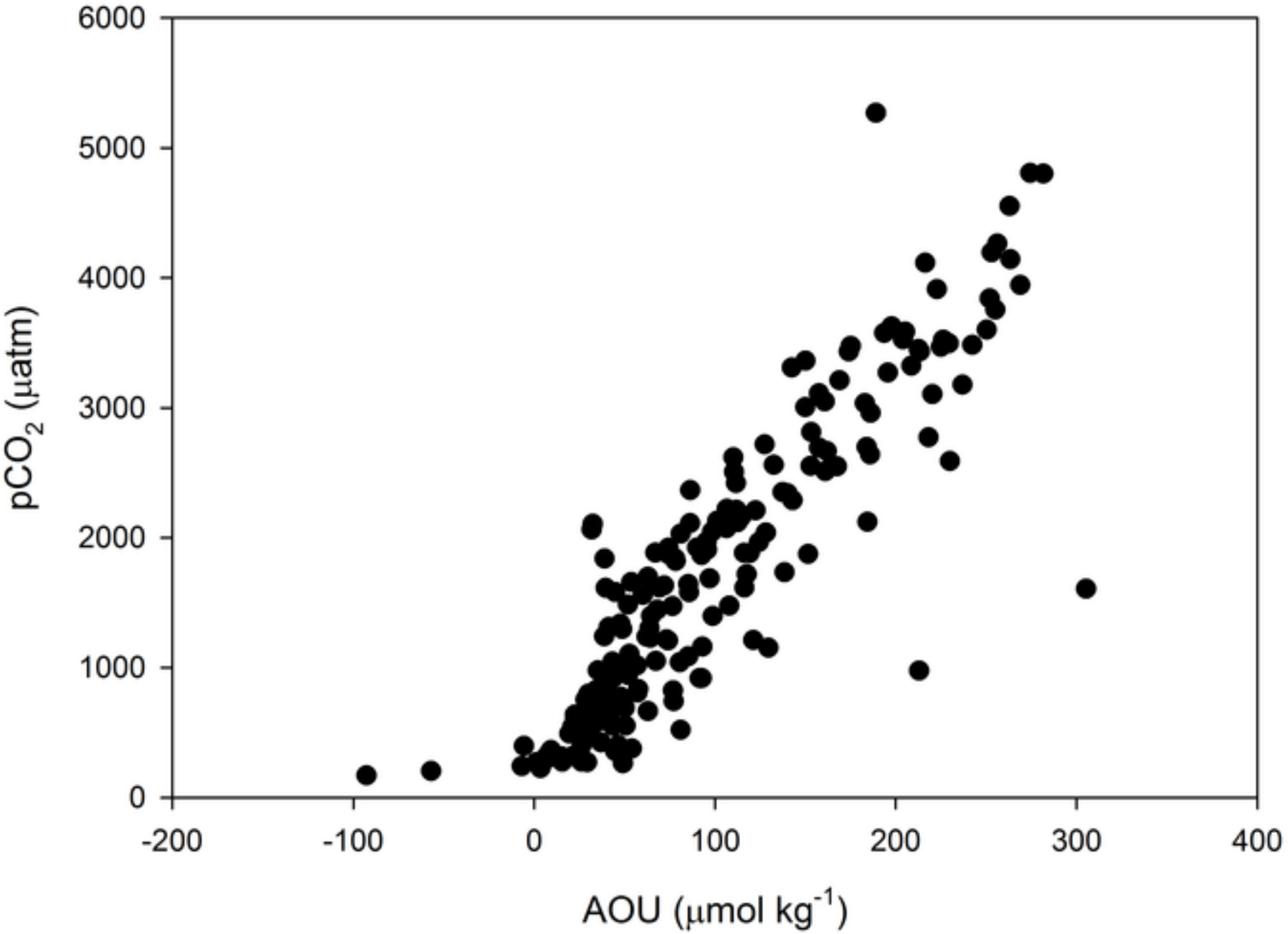

Figure8
Click here to download high resolution image

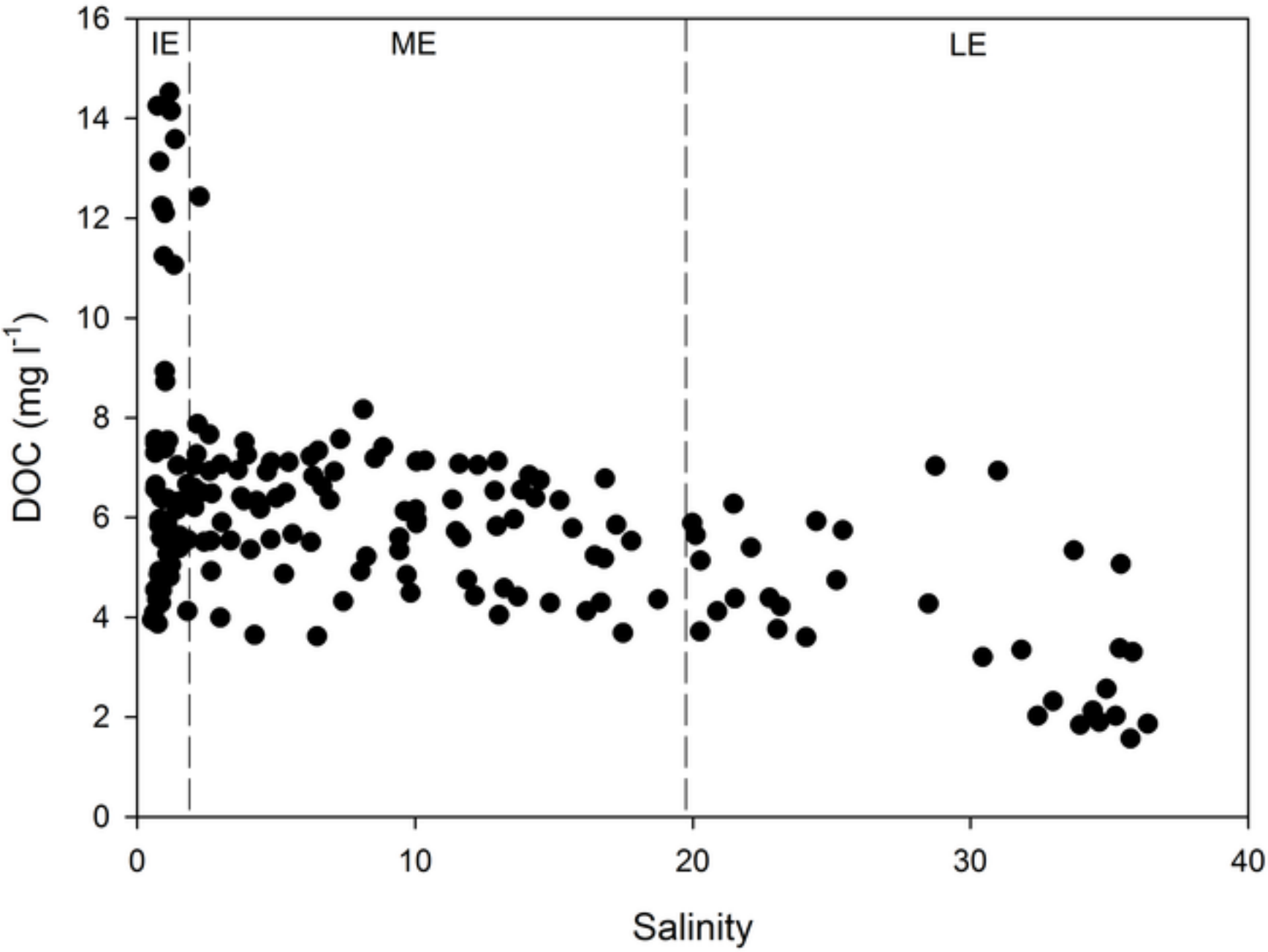

Figure9

Click here to download high resolution image

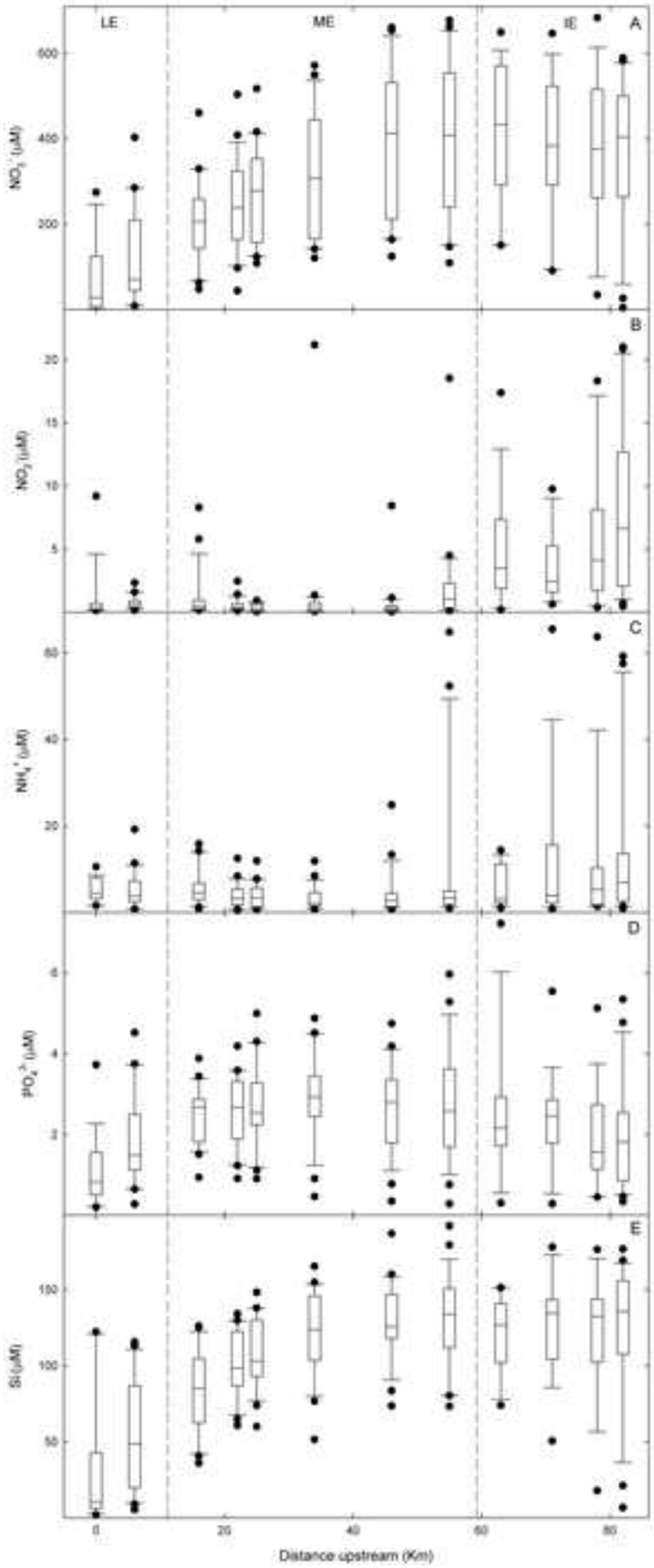

Table1

	Lower estuary	Middle estuary	Inner estuary
Area (km^2)	40.1	23.8	7.2
Temperature (°C)	18.5±4.6	18.2±5.3	19.3±5.8
Salinity	30.0±6.4	9.2±6.8	1.1±0.6
Turbidity (FNU)	111±376	769±1116	310±271
DO ($mg\ l^{-1}$)	6.6±1.0	6.4±1.3	4.0±1.6
pH_{NBS}	8.2±0.1	8.0±0.2	7.8±0.2
A_T ($\mu mol\ kg^{-1}$)	2633±273	3468±403	3505±328
DIC ($\mu mol\ kg^{-1}$)	2613±285	3442±389	3523±300
pCO_2 (ppm)	477±319	1440±807	3009±958
PO_4^{3-} (µM)	1.5±1.1	2.7±1.0	2.2±1.4
Si (µM)	42.5±38.0	112.5±30.3	122.7±36.3
NO_3^- (µM)	99.0±103.3	302.8±154.9	390.3±162.4
NO_2^- (µM)	0.9±1.5	1.1±2.6	5.9±5.4
NH_4^+ (µM)	5.3±3.6	5.2±8.3	19.1±49.4
DOC ($mg\ l^{-1}$)	3.8±1.7	6.0±1.6	6.9 ±2.8
DON ($mg\ l^{-1}$)	15.1±21.7	61.8±56.8	92.6±90.6
Chl*a* ($\mu g\ l^{-1}$)	2.9±3.2	1.8 ±1.4	3.3±3.5
SPM($mg\ l^{-1}$)	771±504	779±790	360±372
PIM ($mg\ l^{-1}$)	667±473	679±708	310±355
POM ($mg\ l^{-1}$)	104±44	100±199	50±43
Kd (m^{-1})	55.9±38.0	57.9±57.5	26.6±27.5

Table2

	Winter	Spring	Summer	Autumn
pH_{NBS}	7.9±0.1	8.1±0.2	8.1±0.1	8.0±0.1
A_T (μmol kg^{-1})	3256±513	3114±658	3185±590	3280±572
DIC (μmol kg^{-1})	3291±520	3095±661	3120±561	3290±584
pCO_2 (μatm)	2063±862	1489±651	1216±387	1924±780

Table3

Zone	Winter flux (mmol C m^{-2} d^{-1})	Spring flux (mmol C m^{-2} d^{-1})	Summer flux (mmol C m^{-2} d^{-1})	Autumn flux (mmol C m^{-2} d^{-1})	Total (mmol C m^{-2} d^{-1})	Annual flux (mol C m^{-2} yr^{-1})
LE	12.6±18.7	-0.7±6.9	0.6±3.0	1.0±3.8	3.4±8.1	1.2±0.6
ME	44.5±25.7	28.1±23.8	15.0±10.6	30.2±21.2	29.4±20.3	10.7±1.1
IE	83.9±31.0	60.2±21.0	43.4±10.5	80.2±12.0	66.9±18.6	24.4±1.7
TOTAL	47.0±35.7	29.2±30.5	19.7±21.7	37.1±40.0	99.7±31.9	36.4±11.7